ACS Medicinal Chemistry Letters

pubs.acs.org/acsmedchemlett Letter

NHC-Ag(I) and NHC-Au(I) Complexes with *N*-Boc-Protected α-Amino Acidate Counterions Powerfully Affect the Growth of MDA-MB-231 Cells

Domenico Iacopetta, Chiara Costabile, Marina La Chimia, Annaluisa Mariconda,* Jessica Ceramella,* Domenica Scumaci, Alessia Catalano, Camillo Rosano, Giovanni Cuda, Maria Stefania Sinicropi,‡ and Pasquale Longo‡

Cite This: *ACS Med. Chem. Lett.* 2023, 14, 1567−1575 Read Online

ACCESS | Metrics & More | Article Recommendations | Supporting Information

ABSTRACT: *N*-Heterocyclic carbene (NHC) metal complexes are attracting scientists' interest as an alluring class of metallodrugs. Indeed, the versatile functionalization of NHC ligands makes them optimal scaffolds to be developed in medicinal chemistry. Besides, amino acids are great biological ligands for metals, such as silver and gold, even though their use is still under-investigated. Aiming to shed light on the anticancer properties of this kind of complex, we investigated a series of silver and gold complexes, stabilized by NHC ligands and bearing carboxylate salts of *tert*-butyloxycarbonyl (Boc)-*N*-protected glycine and L-phenylalanine as anionic ligands. The most active complexes, **AuM1Gly** and **AuM1Phe**, powerfully affect the growth of MDA-MB-231 breast cancer cells, with IC_{50} values in the low nanomolar range. Further studies demonstrated the blockade of the human topoisomerase I activity and actin polymerization reaction at 0.001 μM. These unique features make these complexes very interesting and worthy to be used for future *in vivo* studies.

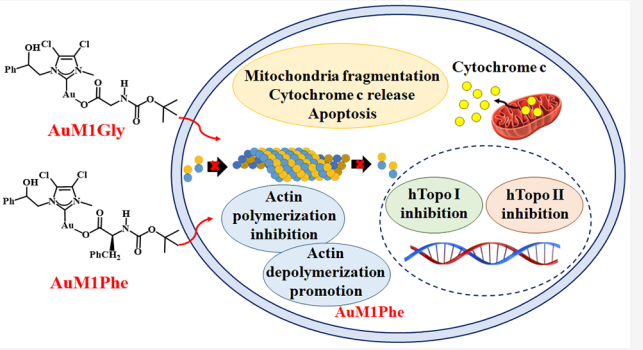

KEYWORDS: *NHC complexes, amino acidate ligands, anticancer activity, human topoisomerases, actin dynamics*

Since the discovery of the antiproliferative activity of cisplatin and its wide clinical use, there has been a considerable interest in the scientific search for transition metal-based anticancer drugs.[1] In the past years, an increasing number of *N*-heterocyclic carbene (NHC) complexes have been developed, and, particularly, NHC-Ag and NHC-Au complexes were proved to be versatile tools.[2] In recent years, we achieved promising results regarding the anticancer properties of several Ag and Au complexes with asymmetrically substituted NHC ligands.[3−8] In Figure 1, the structures of the most promising Ag- and Au-based complexes are reported. Particularly, AuL20[4] exhibited IC_{50} values of 1 μM (95% CI = 0.8−1.2) and 2.6 μM (95% CI = 2.2−3.2) on MCF-7 and ZR-75-1 breast cancer cells, respectively, while AgM1 and AuM1[6] were the most active against the MDA-MB-231 cancer cells, with IC_{50} values of 3.22 ± 1.2 and 2.1 ± 0.7 μM, respectively.

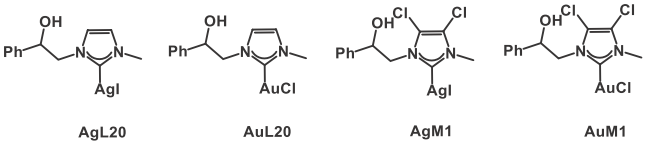

Figure 1. NHC-Ag(I) and NHC-Au(I) complexes previously synthesized.

Besides NHCs, other classes of ligands were used, such as phosphines, thiolates, pyridines, amino acids, and peptides.[9] Recently, some Ag and Au complexes stabilized by NHC ligands and bearing carboxylate salts of *tert*-butyloxycarbonyl (Boc)-*N*-protected amino acids as anionic ligands (Figure 2) were synthesized, characterized, and demonstrated to induce a significant cell disaggregation, after 24 h, using a 3D MeWo cell culture.[10] In this work, different cancer cell models, *viz.*, two breast and two uterine cancer cell lines and two different normal cell lines, MCF-10A and Hek-293 cells, were adopted in order to gain data about the selectivity of the complexes. We obtained thrilling IC_{50} values in the low nanomolar range with high selectivity against the more aggressive and metastatic MDA-MB-231 cells. Moreover, we demonstrated that human

Received: August 14, 2023
Accepted: October 5, 2023
Published: October 10, 2023

https://doi.org/10.1021/acsmedchemlett.3c00360
ACS Med. Chem. Lett. 2023, 14, 1567−1575

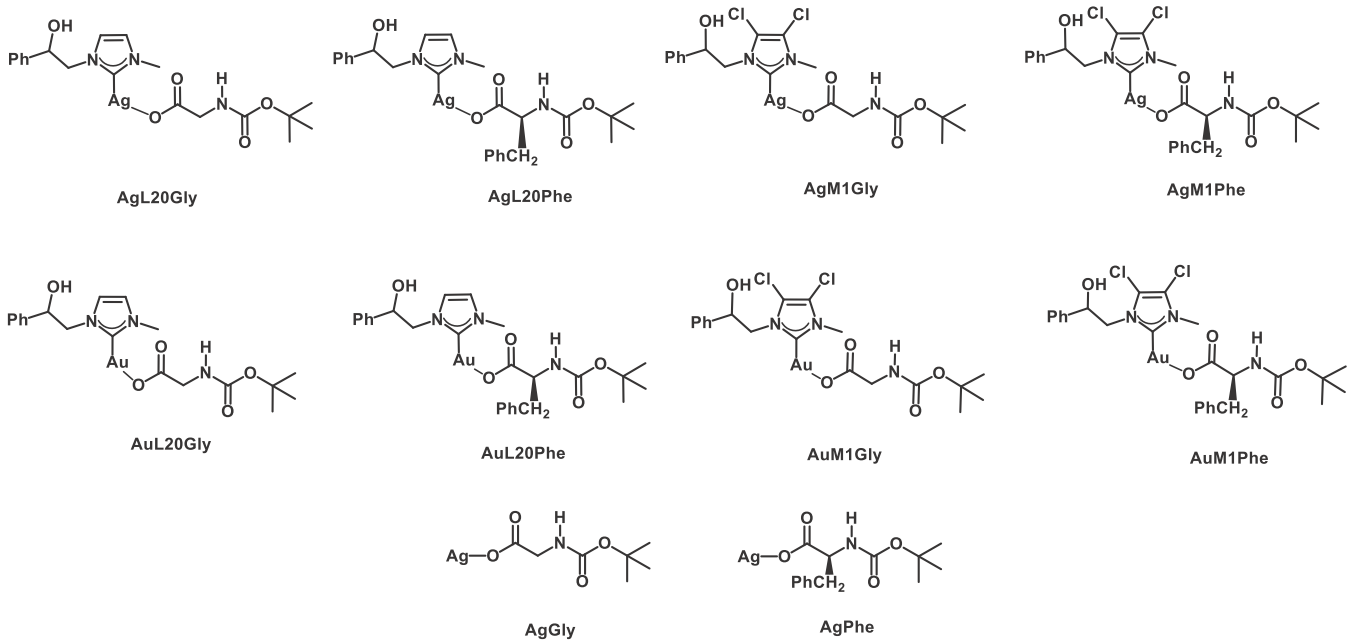

Figure 2. Chemical structures of the silver and gold complexes tested in this work.

Scheme 1. Synthesis of Silver and Gold Complexes Using Amino Acid Anionic Ligands

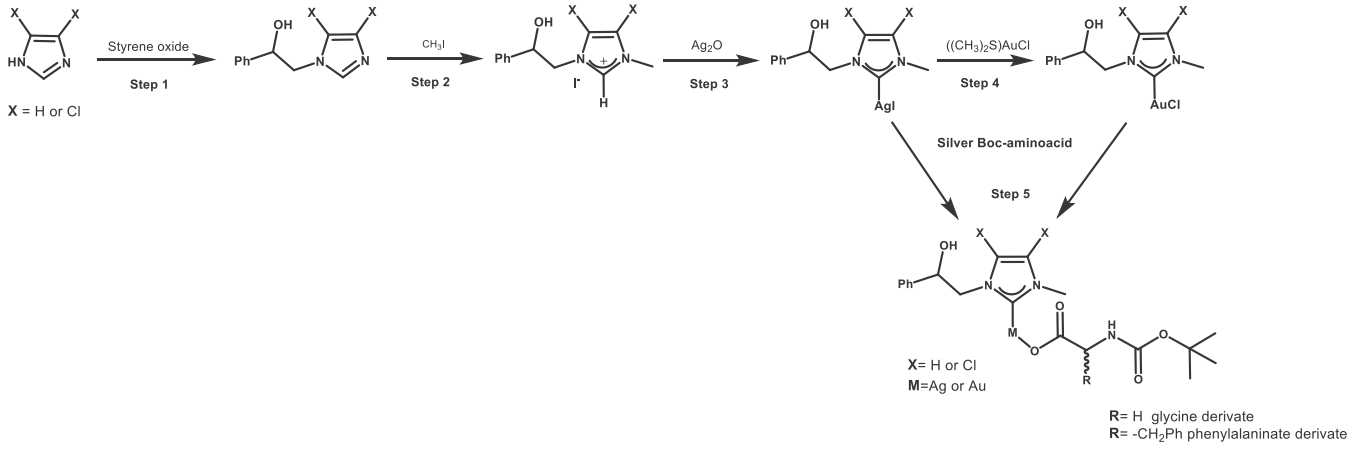

topoisomerase I and actin were involved, being regulated already at a concentration of 0.001 μM. Our outcomes strongly suggest a future development of the two leads, **AuM1Gly** and **AuM1Phe**, as promising scaffolds to be further modified in their chemical structure and, as well, for *in vivo* and preclinical studies.

The structures of transition metal−α-amino acid complexes are illustrated in Figure 2. The NHC ligand *N*-methyl-*N*′-(2-hydroxy-2-phenylethyl)imidazol-2-ylidine is a racemic mixture, and the amino acid derivatives used in these syntheses were Boc-glycinate and Boc-L-phenylalaninate. The anticancer activities of the *N*-Boc-glycinate and *N*-Boc-phenylalaninate complexes were compared with those of silver-Boc-glycinate (AgGly) and silver-Boc-phenylalaninate (AgPhe), reported in Figure 2.

The silver and gold complexes (Figure 2) were prepared following the reported procedure,[10,11] shown in Scheme 1, via the reaction of the appropriate NHC-metal halogenide with 1.2 equiv of *N*-Boc-protected amino acid. The products were obtained after filtration on Celite to remove the insoluble silver halogenide, followed by evaporation of the solvent under reduced pressure. The yields were between 50 and 70%.

The structures of all synthesized products were confirmed by ^{1}H and ^{13}C NMR spectroscopy, elemental analysis, and mass analysis. ^{1}H and ^{13}C NMR spectra recorded in DMSO-d_6 at room temperature substantiated the exchange of the counterion by signals attributable to the *tert*-butyloxycarbonyl group. The resonances of methyl protons of the Boc group were around 1.3−1.4 ppm, those of methyl carbons were around 27−28 ppm, and those of quaternary carbons were about 77 ppm. The ^{13}C NMR spectra of all the tested complexes showed a shift of their carbene carbons to a higher field with respect to the signals of halogenide complexes.[3,4,10,12] Finally, the complexes were thermally and hydrolytically stable. In fact, thermogravimetric analyses showed that they were stable up to temperatures around 150 °C and decomposed before melting. By NMR analyses of complexes in a 90/10 solution of DMSO-d_6/D_2O, no degradation was observed, even after 72 h.

The cytotoxic activity of the complexes was tested against two breast cancer cell lines, MCF-7 and MDA-MB-231, two uterine carcinoma cell lines, HeLa and Ishikawa, and two

https://doi.org/10.1021/acsmedchemlett.3c00360
ACS Med. Chem. Lett. 2023, 14, 1567−1575

Table 1. IC_{50} Values of Silver and Gold Complexes and Cisplatin Expressed[a]

	$IC_{50}(\mu M)$					
	MDA-MB-231	MCF-7	HeLa	Ishikawa	Hek-293	MCF10A
AgGly	4.3 (±1.0) × 10^{-2}	35.7 ± 0.8	21.5 ± 1.6	24.8 ± 1.0	22.3 ± 1.1	>40
AgPhe	3.1 (±0.8) × 10^{-2}	>40	11.9 ± 1.0	28.8 ± 1.2	24.2 ± 1.3	>40
AgL20Gly	2.3 (±0.8) × 10^{-2}	28.9 ± 1.2	11.1 ± 1.0	13.2 ± 0.7	17.9 ± 1.3	>40
AgL20Phe	9.7 (±1.5) × 10^{-2}	24.2 ± 0.8	10.8 ± 1.2	13.4 ± 0.8	11.0 ± 1.2	>40
AuL20Gly	1.8 (±0.4) × 10^{-2}	16.9 ± 1.1	27.2 ± 0.7	13.4 ± 0.9	>40	19.7 ± 0.8
AuL20Phe	1.6 (±0.5) × 10^{-2}	24.3 ± 0.7	21.2 ± 0.3	17.9 ± 0.8	27.4 ± 0.9	>40
AgM1Gly	5.9 (±0.9) × 10^{-2}	28.0 ± 1.3	11.3 ± 0.9	12.2 ± 1.4	11.1 ± 0.7	>40
AgM1Phe	3.8 (±0.7) × 10^{-2}	30.6 ± 1.3	10.7 ± 1.2	10.3 ± 1.1	10.6 ± 1.2	>40
AuM1Gly	1.9 (±0.5) × 10^{-3}	8.9 ± 0.9	8.4 ± 0.8	4.3 ± 1.1	>40	28.6 ± 1.0
AuM1Phe	1.2 (±0.3) × 10^{-2}	4.6 ± 0.9	6.1 ± 0.9	2.7 ± 0.9	15.3 ± 0.9	8.9 ± 1.2
Cisplatin	33.8 ± 1.5	24.9 ± 1.2	16.8 ± 1.6	16.1 ± 1.3	>40	15.7 ± 0.9

[a]The mean ± standard deviations are shown.

Table 2. Selectivity Index (SI) of Silver and Gold Complexes and Cisplatin

	SI							
	MDA-MB-231		MCF-7		HeLa		Ishikawa	
	Hek-293	MCF10A	Hek-293	MCF10A	Hek-293	MCF10A	Hek-293	MCF10A
AgGly	518.6	>930.2	0.6	>1.1	1.0	>1.9	>3.7	>1.6
AgPhe	780.6	>1290.3	>0.6	>1.0	2.0	>3.4	0.8	>1.4
AgL20Gly	778.3	>1739.1	0.6	>1.4	1.61	>3.6	1.4	>3.0
AgL20Phe	113.4	>412.4	0.4	>1.6	1.0	>3.7	0.8	>3.0
AuL20Gly	2222.2	1094.4	>2.4	1.2	1.5	0.7	>3.0	1.5
AuL20Phe	1712.5	>2500.0	1.1	>1.6	1.3	>1.9	1.5	>2.2
AgM1Gly	188.1	>677.9	0.4	>1.4	1.0	>3.5	0.9	>3.3
AgM1Phe	27.9	>105.3	0.3	>1.3	1.0	>3.7	1.0	>3.9
AuM1Gly	>21052.6	15052.6	>4.5	3,2	>4.8	3.4	>9.3	6.6
AuM1Phe	1275.0	741.7	3.3	1.9	2.5	1.5	5.7	3.3
Cisplatin	>1.2	0.5	>1.6	0.6	>2.4	0.9	>2.5	1.0

normal cell lines, the human mammary epithelial MCF-10A and embryonic kidney epithelial Hek-293 cells, by means of the MTT assay. The obtained IC_{50} values, summarized in Table 1, indicated a high to moderate activity against all the cancer cells, ranging from nanomolar to micromolar concentrations. Particularly, all the tested complexes were highly toxic against the MDA-MB-231 cell line (Table 1), and the most active were **AuM1Gly** and **AuM1Phe**, exhibiting IC_{50} values of 1.9 (±0.5) × 10^{-3} and 1.2 (±0.3) × 10^{-2} μM, respectively. The corresponding silver complexes, **AgM1Gly** and **AgM1Phe**, exhibited IC_{50} values of 5.9 (±0.9) × 10^{-2} and 3.8 (±0.7) × 10^{-2} μM, respectively, but they were almost 30 and 3 times, respectively, less potent than the above-mentioned two gold complexes. The remaining gold complexes, **AuL20Gly** and **AuL20Phe**, showed good cytotoxic activities (1.8 (±0.4) × 10^{-2} and 1.6 (±0.5) × 10^{-2} μM, respectively), very close each other. The two corresponding silver complexes, **AgL20Gly** and **AgL20Phe**, and also **AgGly** and **AgPhe**, showed higher IC_{50} values of 2.3 (±0.8) × 10^{-2}, 9.7 (±1.5) × 10^{-2}, 4.3 (±1.0) × 10^{-2}, and 3.1 (±0.8) × 10^{-2} μM, respectively. A similar trend was recorded in the other cancer cell lines used, even though the IC_{50} values fall in the micromolar range. Again, **AuM1Gly** and **AuM1Phe** were the most active, overall (Table 1). Regarding the other complexes, a general trend was noticed, with some exceptions, showing higher activity against the uterine cancer cell lines than against MCF-7 cells. However, **AuM1Gly** and **AuM1Phe** displayed IC_{50} values very near to each other with respect to MCF-7, HeLa, and Ishikawa cancer cells. Moreover, the cytotoxic activity against the two normal cell lines adopted in these assays was low or null (Table 1). Almost all the complexes exhibited a comparable or lower activity with respect to that of cisplatin, adopted as the reference molecule. Importantly, the activity of all complexes against MDA-MB-231 cells was higher than that of cisplatin. The **AuM1Gly** and **AuM1Phe** IC_{50} values for MDA-MB-231 cells were almost 18 000 and 3000 times lower than that of cisplatin, respectively. In any case, they were more active against the other cell lines with respect to cisplatin. Finally, cisplatin exhibited a higher cytotoxic effect against normal human mammary epithelial MCF-10A (IC_{50} = 15.7 ± 0.9 μM), in comparison with most of the other complexes tested.

Finally, the selectivity index (SI) for each studied complex was calculated (Table 2). Almost all tested complexes showed a higher SI compared to cisplatin, and, most importantly, with **AuM1Gly** and **AuM1Phe** the selectivity is extraordinarily higher, overall, and mainly for MDA-MB-231 cells.

In light of the extraordinary activity of **AuM1Gly**, the minimum energy structure was located and is shown in Figure 3 (the *tert*-butyl of the N-Boc-glycinate fragment was simulated as a methyl group). The glycinate fragment is strongly bound to the metal, not only due to the Au−O interaction of gold with the carboxylate (d_{Au-O} = 2.07 Å) but also for the strong hydrogen bond of the second carboxylate oxygen and the hydroxy hydrogen of the NHC ligand (d_{O-H} = 1.88 Å). In addition, the hydrogen-bonding interaction between the same

https://doi.org/10.1021/acsmedchemlett.3c00360
ACS Med. Chem. Lett. 2023, 14, 1567−1575

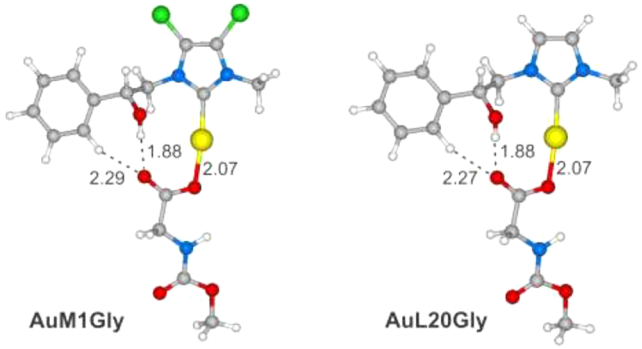

Figure 3. Minimum energy structures of **AuM1Gly** and **AuL20Gly**. Distances are given in Å.

oxygen and the phenyl hydrogen of the ligand is not negligible (d_{O-H} = 2.29 Å). As a consequence of this strong interaction, we found a bond dissociation energy (BDE) calculated in water for the glycinate fragment of 51.7 kcal/mol, significantly higher with respect to the BDE of chlorine in **AuM1** (BDE_{Au-Cl} = 39.2 kcal/mol). Taking into account that the BDE of the glycinate fragment can be also influenced by the chlorines on the NHC backbone, we modeled the corresponding hydrogen-substituted NHC **AuL20Gly** (Figure 3). As expected, a slightly lower BDE (50.5 kcal/mol) was observed for **AuL20Gly**.

The strong interaction between the NHC-Au fragment and glycinate indicates a high stability of **AuM1Gly**. As generally accepted, NHC-Au-X complexes in solution are often in equilibrium with their ionic form, $[Au(NHC)_2]^+[AuX_2]^-$.[13] Considering that this equilibrium can be influenced by the stability of the neutral species NHC-Au-X, we calculated the free energy difference in water between neutral **AuM1Gly** and its ionic form, $[Au(M1)_2]^+[AuGly_2]^-$. The exceptional stability of the neutral form (Figure 3) is confirmed by ΔG = −11.1 kcal/mol with respect to the ionic form. This free energy difference is significantly negative if compared with the analogous ΔG for the corresponding chloride complex **AuM1** (−8.4 kcal/mol). Thus, we can conclude that the exceptional activity of **AuM1Gly** is partially ascribable to the high stability of its neutral form and the strong coordination energy of the glycinate fragment.

In order to study the inhibitory potential of **AuM1Gly** and **AuM1Phe** against the human topoisomerases (hTopos), we performed *in vitro* assays for human topoisomerases I (hTopoI) and II (hTopoII). **AuM1Gly** shows partial inhibition of the hTopoI supercoil relaxing activity at a concentration of 0.001 μM (Figure 4, lane 3). Also shown are the supercoiled (SC) and the relaxed pHOT1 (Figure 4, lanes 1 and 7) and the control reaction (Figure 4, lane 2). On increasing the concentration to 0.01 μM, a full blockade of the enzyme activity was obtained (Figure 4, lane 5). However, **AuM1Phe** totally blocked the hTopoI activity already at the concentration of 0.001 μM and, as well, on increasing the concentration to 0.01 μM (Figure 4, lanes 4 and 6).

Testing the complexes against the hTopoII (Figure 5), no inhibitory activity was recorded at 0.01 and 0.1 μM; indeed, the enzyme retains its full activity (lanes 5 and 6). In lane 4, the control reaction (vehicle) products were loaded. However, by increasing the concentrations to 1 μM, the total blockade of hTopoII activity by both complexes was achieved, as demonstrated by the absence of decatenated products and

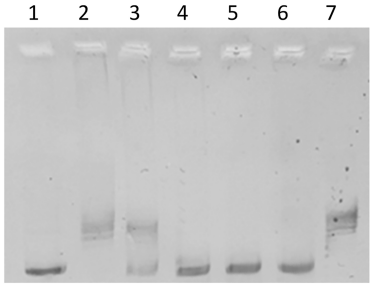

Figure 4. hTopoI relaxation assay: lane 1, SC pHOT1 plasmid; lane 2, CTRL (DMSO); lanes 3 and 5, **AuM1Gly** at 0.001 and 0.01 μM, respectively; lanes 4 and 6, **AuM1Phe** at 0.001 and 0.01 μM, respectively; lane 7, relaxed pHOT1 plasmid.

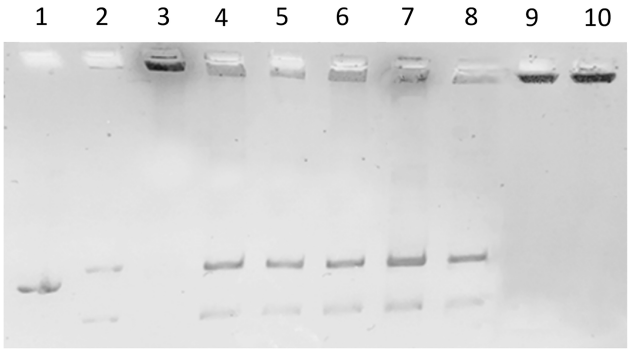

Figure 5. hTopoII decatenation assay: lanes 1−3, linear, decatenated, and catenated kDNA, respectively; lane 4, DMSO; lanes 5 and 6, **AuM1Gly** and **AuM1Phe** at 0.001 μM, respectively; lanes 7 and 8, **AuM1Gly** and **AuM1Phe** at 0.1 μM, respectively; and lanes 9 and 10, **AuM1Gly** and **AuM1Phe** at 1 μM, respectively.

the presence of the interlocked kinetoplast DNA (kDNA) at the gel wells (lanes 9 and 10, **AuM1Gly** and **AuM1Phe**, respectively). Linear, decatenated, and catenated kDNA (Figure 5, lanes 1−3) were used as markers. Thus, both complexes were hTopos inhibitors but with different selectivities, **AuM1Phe** and **AuM1Gly** being 1000 and 100 times more active, respectively, against hTopoI than hTopoII.

The interference with actin dynamics was assessed by using immunostaining evaluations in MDA-MB-231 cells. To that end, cells were exposed to **AuM1Gly** and **AuM1Phe** (at their IC_{50} values) or vehicle (DMSO, negative control) for 24 h. As positive control, we used Latrunculin A (LA, 0.1 μM), a well-known inhibitor.[7,8] The obtained results (Figure 6) suggested a role in actin cytoskeleton destabilization; indeed, MDA-MB-231 cells are smaller and have a round shape (cf. **AuM1Gly** and **AuM1Phe** versus CTRL-vehicle-treated cells, Figure 6B). Both complexes revealed an LA-like arrangement of actin fibers (Figure 6B); the actin cytoskeleton was unevenly distributed and brighter and pooled in thicker structures, with respect to the control (vehicle, Figure 6B). DAPI counterstains for cell nuclei and overlay channels are also shown (Figure 6A,C).

Next, specific *in vitro* actin polymerization and depolymerization experiments were performed. As well in this case, negative (vehicle) and positive (LA and Cytochalasin B, CB) controls were included. In the actin polymerization assay (Figure 7A, CTRL), the control reaction showed a normal actin polymerization curve. Conversely, in the presence of LA or CB (5 μM), there was no increase in RFU values (Figure 7A, LA and CB), as in CTRL. The same behavior was recorded

https://doi.org/10.1021/acsmedchemlett.3c00360
ACS Med. Chem. Lett. 2023, 14, 1567−1575

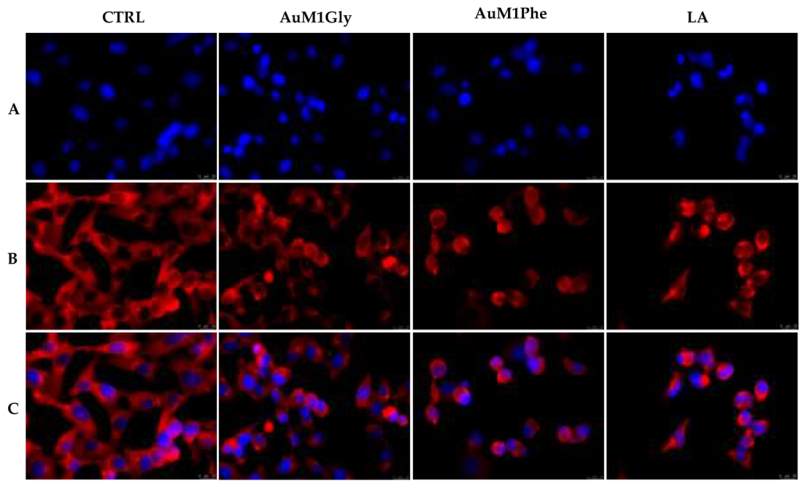

Figure 6. Actin immunostaining performed using MDA-MB-231 cells. After 24 h of exposure to the vehicle (CTRL), LA, **AuM1Gly**, or **AuM1Phe**, cells were subjected to immunostaining, and images were acquired at 40× magnification. (A) DAPI staining ($\lambda_{ex/\lambda em}$ = 350/460 nm); (B) β-actin (Alexa Fluor 568; $\lambda_{ex/\lambda em}$ = 644/665 nm); and (C) merge.

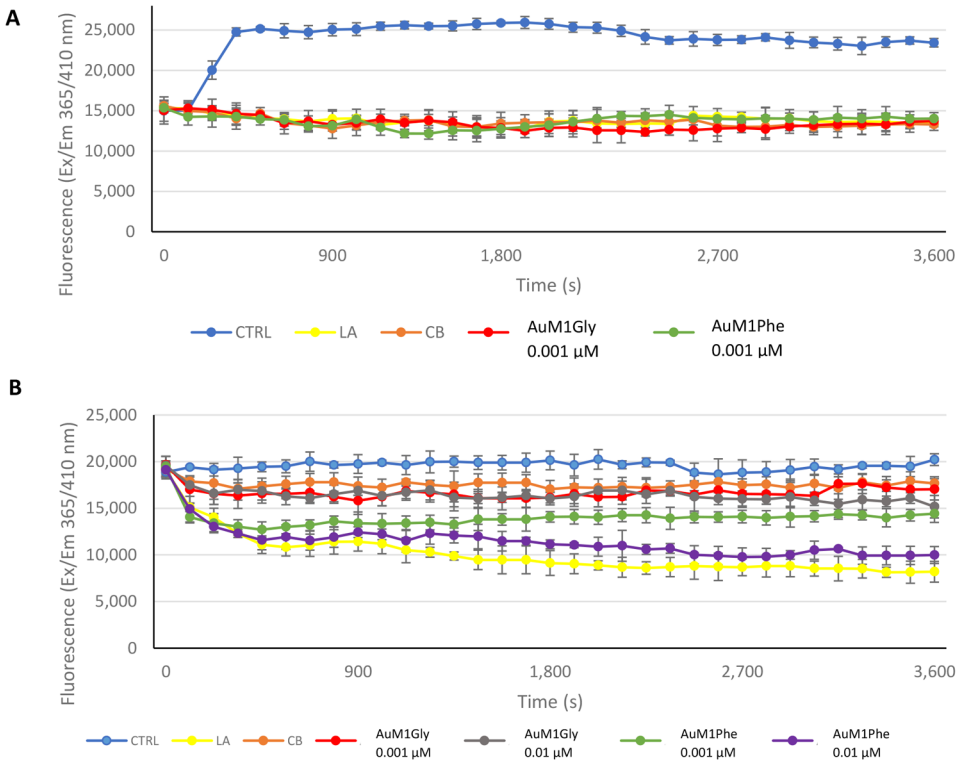

Figure 7. (A) *In vitro* actin polymerization assay. (B) *In vitro* actin depolymerization assay. Vehicle (DMSO), LA and CB (5 μM), and **AuM1Gly** and **AuM1Phe** (0.001 or 0.01 μM).

for **AuM1Gly** and **AuM1Phe**, suggesting that both complexes are actin polymerization inhibitors at 0.001 μM, which is a 5000-fold lower concentration than that adopted for LA and CB. Additionally, LA, but not CB, can also induce the actin filaments (F-actin) depolymerization (Figure 7B). Aiming to determine whether the lead complexes could also have a depolymerizing activity, actin filaments were allowed to form for 1 h, then LA (positive control), CB (negative control), **AuM1Gly**, or **AuM1Phe** was added, and the reactions were monitored for another hour. As visible in Figure 7B, the CTRL, CB, and **AuM1Gly** (at 0.001 and 0.01 μM) curves were similar to each other. A different trend was recorded for LA curve, which decreases rapidly until the final RFU value of about 8.000, due to the F-actin disassembly. Only **AuM1Phe** demonstrated an LA-like activity in a dose dependent manner (see Figure 7B). Indeed at 0.001 μM its curve is positioned between those of CB (negative control) and LA (positive control), but increasing to 0.01 μM, **AuM1Phe** exerted a depolymerizing activity comparable to that of LA. It is important to highlight that the **AuM1Phe** concentration was 500 times lower than that of LA. Summing up, **AuM1Phe** possess an LA-like behavior, whereas **AuM1Gly** inhibits only the F-actin formation, with a CB-like behavior. Both complexes

https://doi.org/10.1021/acsmedchemlett.3c00360
ACS Med. Chem. Lett. 2023, 14, 1567−1575

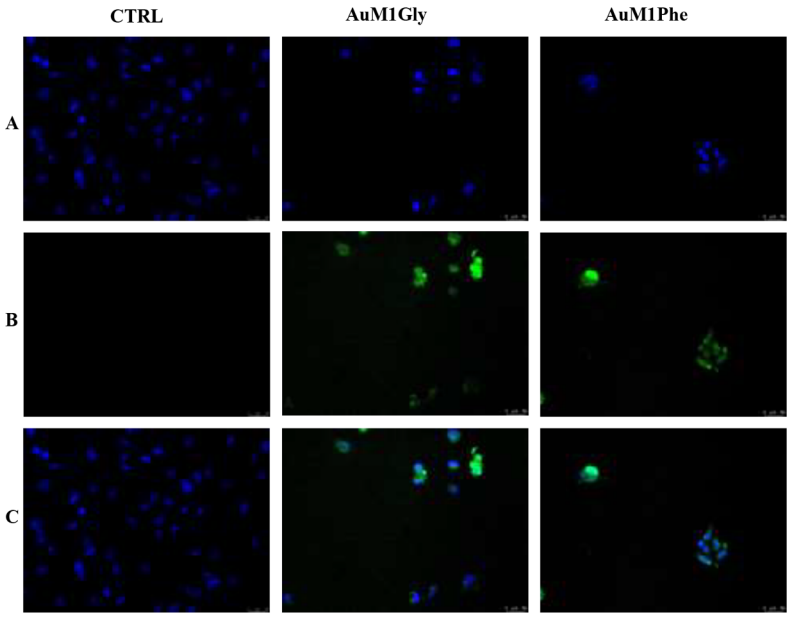

Figure 8. TUNEL assay. MDA-MB-231 cells were treated with vehicle (DMSO, CTRL), **AuM1Gly**, or **AuM1Phe** and then subjected to the assay. (A) DAPI, excitation/emission wavelength 350 nm/460 nm. (B) CF488A, excitation/emission wavelength 490 nm/515 nm. (C) Merge. Images were acquired at 20× magnification.

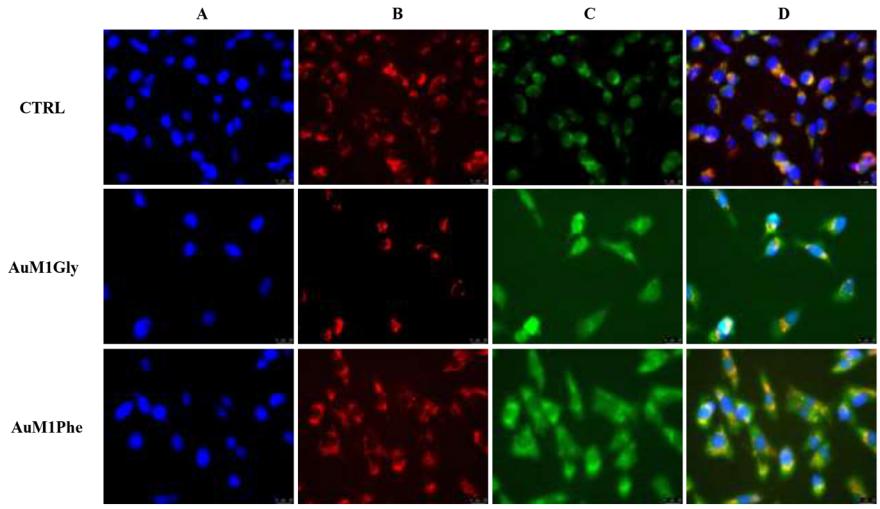

Figure 9. Mitochondria and cytochrome *c* staining. MDA-MB-231 cells were exposed to the vehicle (DMSO, CTRL) or the indicated complexes (24 h, at their IC_{50} values). (A) DAPI nuclear stain (excitation/emission wavelength 350 nm/460 nm). (B) MitoTracker Deep Red FM probe (excitation/emission wavelength 644 nm/665 nm). (C) Alexa Fluor CF 488 (excitation/emission wavelength 490 nm/515 nm). (D) Merge. Images were acquired at 40× magnification.

showed higher potency with respect to the reference molecules.

Next, a TUNEL assay was used to assess the MDA-MB-231 cells death. For this purpose, cells were treated with **AuM1Gly** or **AuM1Phe** at their respective IC_{50} values for 24 h and then further processed. As visible in Figure 8B, both the complexes induced DNA damage, indicated by the green fluorescence visible only within the nuclei of complexes-treated cells but not in the vehicle-treated cells (CTRL, Figure 8B). Nuclei counterstain was obtained using blue DAPI (Figure 8A), and merge channels are also shown (Figure 8C). These findings suggest that both complexes produce DNA damage/fragmentation and force MDA-MB-231 cells to die.

In order to determine whether the complexes induced MDA-MB-231 cells' death by apoptosis, MDA-MB-231 cells were exposed to **AuM1Gly**, **AuM1Phe**, or vehicle and then processed with the MitoTracker Deep Red FM and an anti-cytochrome *c* antibody. The results show a regular location of cytochrome *c* (Figure 9C, CTRL, green fluorescence) within the mitochondrial compartment (Figure 9D, CTRL, red fluorescence) in vehicle-treated cells, as visible in the merge channel (Figure 9D, CTRL). In contrast, under **AuM1Gly** or **AuM1Phe** treatment, cytochrome *c* was found diffusely distributed within the cell cytoplasm, as evidenced by the green fluorescence (Figure 9C), and mitochondria appear destroyed; indeed, the red fluorescence takes punctiform or packed shapes (Figure 9B). Finally, the merge channels

https://doi.org/10.1021/acsmedchemlett.3c00360
ACS Med. Chem. Lett. 2023, 14, 1567−1575

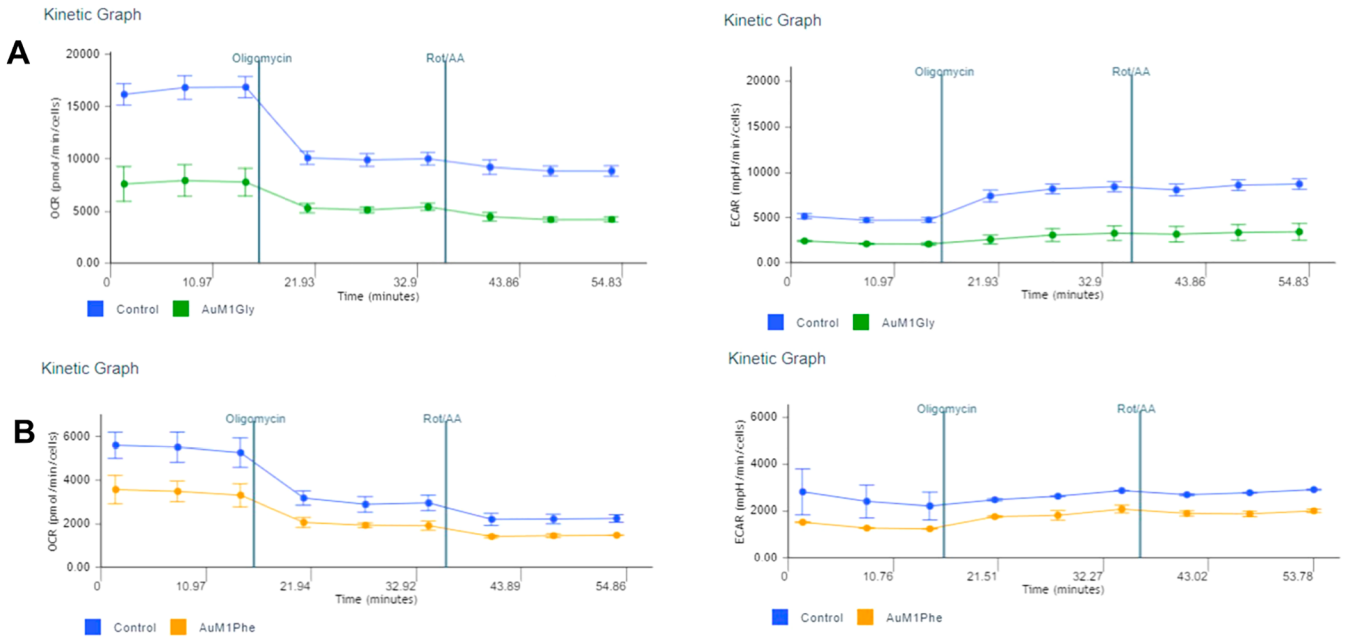

Figure 10. Glycolytic and Oxphos activities were measured by the extracellular acidification rate (ECAR) and the oxygen consumption rate (OCR) in MDA-MB-231 breast cancer cells treated with **AuM1Gly** (A) or **AuM1Phe** (B). The study was done using the miniXFp analyzer. The analysis unveils that the analyzed compounds impact ATP production by impairing both ECAR and OCR.

(Figure 9D) indicate a non-superimposition of cytochrome *c* and mitochondria staining, meaning that the intrinsic apoptotic mechanism took place.[14]

The possible impact on cancer cell bioenergetics in terms of ATP production, with or without complex treatment, was investigated using the Seahorse XF HS mini analyzer. Treatment with **AuM1Gly** or **AuM1Phe** induced a significant reduction of whole ATP production by impairing the oxygen consumption rate (OCR) and/or the extracellular acidification rate (ECAR) with respect to the vehicle-treated cells. As depicted in Figure 10A, the most striking finding is the impact on ATP production, already at a concentration of 0.25 μM, of **AuM1Gly** that decreased both the ECAR and OCR. **AuM1Phe** also produced a significant effect, but with a lower activity, detectable at a concentration of 1 μM, and with a higher specificity in impairing the OCR-generated ATP. Therefore, **AuM1Gly** regulates the glycolytic and oxidative ATP production rates, whereas **AuM1Phe** principally impacts the oxidative metabolism.

Summing up, the individuated leads are thermally, energetically, and hydrolytically stable and possess an extraordinary anticancer activity against the MDA-MB-231 cancer cells. These results may depend on different reasons, such as the continuous supply of nutrients, among them amino acids,[15] needed for the uncontrolled cancer cells' growth and progression. Moreover, glycine and phenylalanine transporters are often overexpressed,[16] mostly in the highly malignant and metastatic MDA-MB-231 cells. Thus, we can speculate that the extraordinary activity may be due, in part, to a higher influx and stability of **AuM1Gly**. NHC-Ag and NHC-Au complexes became fruitful scaffolds in medicinal chemistry and were proved to target different and vital proteins involved in cancer onset and progression, such as thioredoxin reductase, ubiquitin−proteasome, tyrosine kinases, topoisomerase, and so on.[17]

Studies conducted on several gold and silver complexes indicated topoisomerases as interesting targets,[18] even though with very different inhibiting concentrations and mechanisms. In this case, the two leads inhibited both the hTopos but with a net selectivity against hTopoI, particularly **AuM1Phe** at the extraordinary concentration of 0.001 μM. This strong inhibition is, to our best knowledge, a unique feature among the numerous reported metal complexes and even better with respect to the well-known hTopos inhibitors.[19−22] Furthermore, the ability to block F-actin formation was proved at 0.001 μM, which is a considerably lower concentration than required with the well-known inhibitors, such as CB, LA, Cytochalasin D, and others.[23−27] Additionally, **AuM1Phe** behaved like LA in promoting the F-actin depolymerization, but with a higher activity with respect to LA and other actin depolymerization promoters.[25,27,28] These features greatly impact the MDA-MB-231 cancer cells' bioenergetics, causing their death by the intrinsic apoptotic mechanism. We are confident that the presented outcomes could represent the main road from which multiple secondary roads branch off, leading to a deeper comprehension of the important role of NHC−amino acid−metal complexes in cancer therapy.

■ ASSOCIATED CONTENT

Supporting Information

The Supporting Information is available free of charge at https://pubs.acs.org/doi/10.1021/acsmedchemlett.3c00360.

Experimental details: cell culture, cell viability assays, human topoisomerase I relaxation assay, human topoisomerase II decatenation assay, mitochondrial staining and immunofluorescence, actin polymerization/depolymerization assay, TUNEL assay, seahorse XF HS mini analyzer, statistical analysis, and safety statement (PDF)

https://doi.org/10.1021/acsmedchemlett.3c00360
ACS Med. Chem. Lett. 2023, 14, 1567−1575

AUTHOR INFORMATION

Corresponding Authors

Annaluisa Mariconda − *Department of Science, University of Basilicata, 85100 Potenza, Italy;* orcid.org/0000-0002-9763-838X; Email: annaluisa.mariconda@unibas.it

Jessica Ceramella − *Department of Pharmacy, Health and Nutritional Sciences, University of Calabria, 87036 Arcavacata di Rende, Italy;* orcid.org/0000-0002-1386-3601; Email: jessica.ceramella@unical.it

Authors

Domenico Iacopetta − *Department of Pharmacy, Health and Nutritional Sciences, University of Calabria, 87036 Arcavacata di Rende, Italy;* orcid.org/0000-0001-5179-7118

Chiara Costabile − *Department of Chemistry and Biology "A. Zambelli", University of Salerno, 84084 Fisciano, SA, Italy;* orcid.org/0000-0001-8538-7125

Marina La Chimia − *Laboratory of Proteomics, Department of Experimental and Clinical Medicine and Research Center on Advanced Biochemistry and Molecular Biology, Magna Græcia University of Catanzaro, 88100 Catanzaro, Italy*

Domenica Scumaci − *Laboratory of Proteomics, Department of Experimental and Clinical Medicine and Research Center on Advanced Biochemistry and Molecular Biology, Magna Græcia University of Catanzaro, 88100 Catanzaro, Italy;* orcid.org/0000-0002-8117-834X

Alessia Catalano − *Department of Pharmacy−Drug Sciences, University of Bari Aldo Moro, 70126 Bari, Italy*

Camillo Rosano − *U.O. Proteomica e Spettrometria di Massa, IRCCS Ospedale Policlinico San Martino, 16132 Genova, Italy*

Giovanni Cuda − *Laboratory of Proteomics, Department of Experimental and Clinical Medicine and Research Center on Advanced Biochemistry and Molecular Biology, Magna Græcia University of Catanzaro, 88100 Catanzaro, Italy*

Maria Stefania Sinicropi − *Department of Pharmacy, Health and Nutritional Sciences, University of Calabria, 87036 Arcavacata di Rende, Italy*

Pasquale Longo − *Department of Chemistry and Biology "A. Zambelli", University of Salerno, 84084 Fisciano, SA, Italy*

Complete contact information is available at: https://pubs.acs.org/10.1021/acsmedchemlett.3c00360

Author Contributions

‡M.S.S. and P.L. contributed equally to this work.

Funding

M.S.S. was supported by PON "R&I" 2014−2020 project from Area di Specializzazione "Salute", ARS01_00568 titled "SI.F.I.PA.CRO.DE.−Sviluppo e industrializzazione farmaci innovativi per terapia molecolare personalizzata PA. CRO.DE" for providing lab tools. This work was supported by PRIN 2022, Code 2022HARH5W − HyMTA (Hybrid Multi-Target Agents) (CUP MASTER: C53D23004490001).

Notes

The authors declare no competing financial interest.

ABBREVIATIONS

NHC, *N*-heterocyclic carbene; Boc, *tert*-butyloxycarbonyl; NMR, nuclear magnetic resonance; DMSO, dimethyl sulfoxide; IC_{50}, 50% inhibitory concentration; SI, selectivity index; BDE, bond dissociation energy; hTopos, human topoisomerases; SC, supercoiled; kDNA, kinetoplast deoxyribonucleic acid; LA, latrunculin A; CB, cytochalasin B; DAPI, 4′,6-diamidino-2-phenylindole; CTRL, control; RFU, relative fluorescence unit; Ex/Em, excitation/emission; OCR, oxygen consumption rate; ECAR, extracellular acidification rate; ATP, adenosine triphosphate

REFERENCES

(1) Ceramella, J.; Mariconda, A.; Iacopetta, D.; Saturnino, C.; Barbarossa, A.; Caruso, A.; Rosano, C.; Sinicropi, M. S.; Longo, P. From coins to cancer therapy: Gold, silver and copper complexes targeting human topoisomerases. *Bioorg. Med. Chem. Lett.* **2020**, *30* (3), 126905.

(2) Jalal, M.; Hammouti, B.; Touzani, R.; Aouniti, A.; Ozdemir, I. Metal-NHC heterocycle complexes in catalysis and biological applications: Systematic review. *Mater. Today: Proc.* **2020**, *31*, S122−S129.

(3) Napoli, M.; Saturnino, C.; Sirignano, E.; Popolo, A.; Pinto, A.; Longo, P. Synthesis, characterization and cytotoxicity studies of methoxy alkyl substituted metallocenes. *Eur. J. Med. Chem.* **2011**, *46* (1), 122−128.

(4) Saturnino, C.; Barone, I.; Iacopetta, D.; Mariconda, A.; Sinicropi, M. S.; Rosano, C.; Campana, A.; Catalano, S.; Longo, P.; Andò, S. N-heterocyclic carbene complexes of silver and gold as novel tools against breast cancer progression. *Fut. Med. Chem.* **2016**, *8* (18), 2213−2229.

(5) Iacopetta, D.; Mariconda, A.; Saturnino, C.; Caruso, A.; Palma, G.; Ceramella, J.; Muià, N.; Perri, M.; Sinicropi, M. S.; Caroleo, M. C.; Longo, P. Novel Gold and Silver Carbene Complexes Exert Antitumor Effects Triggering the Reactive Oxygen Species Dependent Intrinsic Apoptotic Pathway. *ChemMedChem* **2017**, *12* (24), 2054−2065.

(6) Iacopetta, D.; Rosano, C.; Sirignano, M.; Mariconda, A.; Ceramella, J.; Ponassi, M.; Saturnino, C.; Sinicropi, M. S.; Longo, P. Is the Way to Fight Cancer Paved with Gold? Metal-Based Carbene Complexes with Multiple and Fascinating Biological Features. *Pharmaceuticals* **2020**, *13* (5), 91.

(7) Iacopetta, D.; Ceramella, J.; Rosano, C.; Mariconda, A.; Pellegrino, M.; Sirignano, M.; Saturnino, C.; Catalano, A.; Aquaro, S.; Longo, P.; Sinicropi, M. S. N-Heterocyclic Carbene-Gold(I) Complexes Targeting Actin Polymerization. *Appl. Sci.* **2021**, *11* (12), 5626.

(8) Ceramella, J.; Mariconda, A.; Sirignano, M.; Iacopetta, D.; Rosano, C.; Catalano, A.; Saturnino, C.; Sinicropi, M. S.; Longo, P. Novel Au Carbene Complexes as Promising Multi-Target Agents in Breast Cancer Treatment. *Pharmaceuticals* **2022**, *15* (5), 507.

(9) Andrejević, T. P.; Glišić, B. Đ.; Djuran, M. I. Amino Acids and Peptides as Versatile Ligands in the Synthesis of Antiproliferative Gold Complexes. *Chemistry* **2020**, *2* (2), 203−218.

(10) Ciardulli, M. C.; Mariconda, A.; Sirignano, M.; Lamparelli, E. P.; Longo, R.; Scala, P.; D'Auria, R.; Santoro, A.; Guadagno, L.; Della Porta, G.; Longo, P. Activity and Selectivity of Novel Chemical Metallic Complexes with Potential Anticancer Effects on Melanoma Cells. *Molecules* **2023**, *28* (12), 4851.

(11) Hackenberg, F.; Müller-Bunz, H.; Smith, R.; Streciwilk, W.; Zhu, X.; Tacke, M. Novel Ruthenium(II) and Gold(I) NHC Complexes: Synthesis, Characterization, and Evaluation of Their Anticancer Properties. *Organometallics* **2013**, *32* (19), 5551−5560.

(12) Mariconda, A.; Sirignano, M.; Costabile, C.; Longo, P. New NHC- silver and gold complexes active in A3-coupling (aldehyde-alkyne-amine) reaction. *Mol. Catal.* **2020**, *480*, 110570.

(13) Mariconda, A.; Grisi, F.; Costabile, C.; Falcone, S.; Bertolasi, V.; Longo, P. Synthesis, characterization and catalytic behaviour of a palladium complex bearing a hydroxy-functionalized N-heterocyclic carbene ligand. *New J. Chem.* **2014**, *38* (2), 762−769.

(14) Jan, R.; Chaudhry, G.-e.-S. Understanding Apoptosis and Apoptotic Pathways Targeted Cancer Therapeutics. *Advanced. Pharmaceut. Bull.* **2019**, *9* (2), 205−218.

(15) Cha, Y.; Kim, E.-S.; Koo, J. Amino Acid Transporters and Glutamine Metabolism in Breast Cancer. *Int. J. Mol. Sci.* **2018**, *19* (3), 907.
(16) Noh, S.; Kim, D. H.; Jung, W. H.; Koo, J. S. Expression levels of serine/glycine metabolism-related proteins in triple negative breast cancer tissues. *Tumor Biol.* **2014**, *35* (5), 4457−4468.
(17) Mora, M.; Gimeno, M. C.; Visbal, R. Recent advances in gold−NHC complexes with biological properties. *Chem. Soc. Rev.* **2019**, *48* (2), 447−462.
(18) Baglini, E.; Salerno, S.; Barresi, E.; Robello, M.; Da Settimo, F.; Taliani, S.; Marini, A. M. Multiple Topoisomerase I (TopoI), Topoisomerase II (TopoII) and Tyrosyl-DNA Phosphodiesterase (TDP) inhibitors in the development of anticancer drugs. *Eur. J. Pharmaceut. Sci.* **2021**, *156*, 105594.
(19) Talukdar, A.; Kundu, B.; Sarkar, D.; Goon, S.; Mondal, M. A. Topoisomerase I inhibitors: Challenges, progress and the road ahead. *Eur. J. Med. Chem.* **2022**, *236*, 114304.
(20) Katkar, P.; Coletta, A.; Castelli, S.; Sabino, G. L.; Couto, R. A. A.; da Costa Ferreira, A. M.; Desideri, A. Effect of oxindolimine copper(ii) and zinc(ii) complexes on human topoisomerase I activity. *Metallomics* **2014**, *6* (1), 117−125.
(21) Martín-Encinas, E.; Conejo-Rodríguez, V.; Miguel, J. A.; Martínez-Ilarduya, J. M.; Rubiales, G.; Knudsen, B. R.; Palacios, F.; Alonso, C. Novel phosphine sulphide gold(i) complexes: topoisomerase I inhibitors and antiproliferative agents. *Dalton Trans.* **2020**, *49* (23), 7852−7861.
(22) Xiong, K.; Qian, C.; Yuan, Y.; Wei, L.; Liao, X.; He, L.; Rees, T. W.; Chen, Y.; Wan, J.; Ji, L.; Chao, H. Necroptosis Induced by Ruthenium(II) Complexes as Dual Catalytic Inhibitors of Topoisomerase I/II. *Angew. Chem., Int. Ed.* **2020**, *59* (38), 16631−16637.
(23) Fokin, A. I.; Chuprov-Netochin, R. N.; Malyshev, A. S.; Romero, S.; Semenova, M. N.; Konyushkin, L. D.; Leonov, S. V.; Semenov, V. V.; Gautreau, A. M. Synthesis, Screening and Characterization of Novel Potent Arp2/3 Inhibitory Compounds Analogous to CK-666. *Front. Pharmacol.* **2022**, *13*, 896994.
(24) Yarmola, E. G.; Somasundaram, T.; Boring, T. A.; Spector, I.; Bubb, M. R. Actin-Latrunculin A Structure and Function. *J. Biol. Chem.* **2000**, *275* (36), 28120−28127.
(25) Hori, M.; Yazama, F.; Matsuura, Y.; Yoshimoto, R.; Kaneda, T.; Yasumoto, T.; Ozaki, H.; Karaki, H. Inhibition of actin polymerization by marine toxin pectenotoxin-2. *J. Vet. Med. Sci.* **2018**, *80* (2), 225−234.
(26) Miyazaki, S.; Sasazawa, Y.; Mogi, T.; Suzuki, T.; Yoshida, K.; Dohmae, N.; Takao, K.-i.; Simizu, S. Identification of seco-clavilactone B as a small-molecule actin polymerization inhibitor. *FEBS Lett.* **2016**, *590* (8), 1163−1173.
(27) Usui, T.; Kazami, S.; Dohmae, N.; Mashimo, Y.; Kondo, H.; Tsuda, M.; Terasaki, A. G.; Ohashi, K.; Kobayashi, J. i.; Osada, H. Amphidinolide H, a Potent Cytotoxic Macrolide, Covalently Binds on Actin Subdomain 4 and Stabilizes Actin Filament. *Chem. Biol.* **2004**, *11* (9), 1269−1277.
(28) Futaki, K.; Takahashi, M.; Tanabe, K.; Fujieda, A.; Kigoshi, H.; Kita, M. Synthesis and Biological Activities of Aplyronine A Analogues toward the Development of Antitumor Protein−Protein Interaction Inducers between Actin and Tubulin: Conjugation of the C1−C9Macrolactone Part and the C24−C34 Side Chain. *ACS Omega* **2019**, *4* (5), 8598−8613.

https://doi.org/10.1021/acsmedchemlett.3c00360
ACS Med. Chem. Lett. 2023, 14, 1567−1575